Thermo-micromechanics of strain-induced crystallization

V.N. Khiêm, Jean-Benoit Le Cam, X. Balandraud, M. Itskov

Thermo-micromechanics of strain-induced crystallization

V.N. Khiêm
Department of Continuum Mechanics, RWTH Aachen University, Germany

J.-B. Le Cam
Institut de Physique UMR 6251 CNRS/Université de Rennes 1, Rennes, France

X. Balandraud
Université Clermont Auvergne, CNRS, SIGMA, Institut Pascal, Clermont-Ferrand, France

M. Itskov
Department of Continuum Mechanics, RWTH Aachen University, Germany

ABSTRACT: Strain-induced crystallization in natural rubber has long been modeled as an isothermal process. Recent calorimetric measurements (Samaca Martinez et al. 2013a,b) and a theoretical result (Khiˆem and Itskov 2018) revealed severe limitations of this approach. First, it was not able to describe the Gough-Joule effect as well as the rate of crystallization (melting) in natural rubber. Second, the stress-strain hysteresis of natural rubber was improperly attributed to the mechanical dissipation. In this contribution, we present a fully coupled thermo-micromechanical theory of strain-induced crystallization in natural rubber. Accordingly, deformation is accompanied by heat production/absorption. It potentially induces an evolution of the heat source which alters the temperature of the sample. In contrast to previous works on thermo-mechanics of rubber-like materials, the internal energy and the entropy are formulated in our model explicitly in terms of state variables. The crystallinity is not considered as an internal variable, and its evolution is elucidated by crystal nucleation in loading and crystal growth in unloading. The crystallization kinetics (Khiˆem and Itskov 2018) is further extended beyond uniaxial deformation, which offers microscopic boundary conditions for the representative chain on the one hand, and provides a formulation for the crystallinity on the other hand. Model predictions are compared with comprehensive experimental results and shed new light on strain-induced crystallization of natural rubber.

1 INTRODUCTION

Despite recent efforts on theoretical treatments of the kinetics of strain-induced crystallites in natural rubbers (Laghmach, Candau, Chazeau, & Munch 2015, Plagge & Klüppel 2018, Gros, Huneau, Verron, & Tosaka 2019), thermomechanics of strain-induced crystallization has not been fully understood. Indeed, most of the constitutive models proposed for strain-induced crystallization are isothermal (see counter-examples in Behnke2018 and Khiem 2018b), which contradicts experimental data (Samaca Martinez, Le Cam, Balandraud, Toussaint,& Caillard 2013a). Furthermore, these elastoplasticity-based models predict strictly positive mechanical dissipation, which has not been observed in calorimetric analysis (Samaca Martinez, Le Cam, Balandraud, Toussaint, & Caillard 2013b). For further discussion on constitutive modeling of strain-induced crystallization, interested readers are referred to Khiêm and Itskov (2018b).

In this paper, we propose a fully coupled thermo-micromechanical theory of strain-induced crystallization in natural rubber. The model is constructed on the basis of the analytical network averaging concept (Khiêm & Itskov 2016, Khiêm & Itskov 2018b). Accordingly, microscopic boundary conditions of representative chains are driven by microstructural alteration of natural rubbers due to strain-induced crystallization. The evolution of crystallinity is explained by nucleation of bundle-like crystallites in loading and growth and melting of crystallites under unloading (Khiêm & Itskov 2018b). The proposed theory includes few physically motivated material constants and demonstrates good agreement with full thermal and calorimetric fields measurement of natural rubbers.

2 EXPERIMENTAL SETUP

2.1 *Material, specimen geometry, testing machine and loading conditions*

The material considered here is an unfilled natural rubber. The test was carried out with a cruciform-shaped specimen. Its total length is 125 mm and its

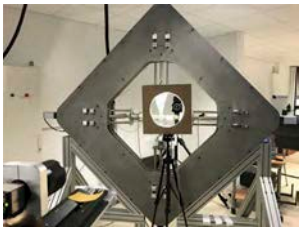

Figure 1. Overview of the experimental setup

thickness is 2 mm. Figure 1 presents an overview of the experimental setup composed of a home-made biaxial testing machine, an infrared (IR) camera and the cruciform-shaped specimen. The machine is composed of four independent electrical actuators controlled by an in-house LabVIEW program. Two load cells measure the force in the two perpendicular directions. The four specimen branches were stretched under a prescribed displacement equal to 200 mm at a rate of 150 mm/min. An optical camera and a home-made LED system can also be seen in the figure. They were used for evaluating the full displacement fields by digital image correlation.

2.2 *Full thermal field measurement*

Temperature measurements were performed by using a FLIR IR camera equipped with a focal plane array of 640 × 512 pixels and detectors operating in wavelengths between 1.5 and 5.1 μm. The integration time and the acquisition frequency were 2623 μs and 5 Hz, respectively. The calibration of camera detectors was performed with a black body using a one-point Non-Uniformity Correction (NUC) procedure at this acquisition frequency. The thermal resolution or noise equivalent temperature difference (NETD) was 20 mK for a temperature range between 5 and 40°C. The spatial resolution of the thermal field was equal to 390 μm/px. The IR camera was switched on several hours before testing in order to ensure its internal temperature to be stabilized.

3 THERMOMECHANICAL FRAMEWORK

3.1 *Helmholtz free energy*

The Helmholtz free energy of natural rubber at a continuum material point can be given in the general case by

$$\Psi = U(\mathbf{F}, \Xi, T) - T\eta(\mathbf{F}, \Xi, T), \tag{1}$$

where U is the internal energy per unit referential volume and η is the network entropy. $\mathbf{F}$ is the deformation gradient, Ξ denotes an internal variable and T is the absolute temperature. The quantities $\mathbf{F}$, Ξ and T are state variables.

3.2 *Laws of thermodynamics*

The local form of the first law of thermodynamics is given in the Lagrangian description by Germain et al. 1983 as

$$\dot{U} = \mathbf{P} : \dot{\mathbf{F}} - \mathrm{Div}Q + \hat{R}, \tag{2}$$

where Q is the heat influx per unit referential area, $\hat{R}$ denotes the heat supply per unit referential volume of the body, $\mathbf{P}$ is the first Piola-Kirchhoff stress tensor and the superposed dot indicates the material time derivative.

The second law of thermodynamics can be given in the form of the Clausius-Planck inequality by Germain et al. 1983 as

$$D_{\text{int}} = \mathbf{P} : \dot{\mathbf{F}} - \dot{U} + T\dot{\eta} \geq 0. \tag{3}$$

Therein, D_{int} is referred to as internal dissipation in Holzapfel (2000, page 170), or as mechanical or intrinsic dissipation in calorimetric studies (see e.g. Chrysochoos et al. (2010)).

In view of (1) and (3), one can write (Khiêm & Itskov 2018b)

$$\mathbf{P} = \frac{\partial U}{\partial \mathbf{F}} - T\frac{\partial \eta}{\partial \mathbf{F}} - p\mathbf{F}^{-\mathrm{T}}, \tag{4}$$

$$\frac{\partial U}{\partial T} = T\frac{\partial \eta}{\partial T}, \tag{5}$$

$$D_{\text{int}} = -\frac{\partial U}{\partial \Xi} : \dot{\Xi} + T\frac{\partial \eta}{\partial \Xi} : \dot{\Xi} \geq 0, \tag{6}$$

where p denotes a Lagrange multiplier arising from the incompressibility constraint. Note that the mass densities of crystalline and amorphous rubber are different, so the volume of natural rubber sample changes during deformation (up to 6%, see e.g. Le Cam and Toussaint (2008)). However for the sake of simplicity, we neglect the change in volume of natural rubber, and consider it as incompressible. In view of (1) and (5), the entropy of the rubber network is given by

$$\eta = -\frac{\partial \Psi}{\partial T}. \tag{7}$$

3.3 *Statistical mechanics of a polymer network*

According to the analytical network averaging concept (Khiêm & Itskov 2016), all polymer chains in the rubber network are replaced by a representative freely jointed chain confined in a mean tube undergoing a microscopic tube stretch and a microscopic tube contraction. The number of microstates the chain can be realized by rotations about its segments

can be calculated via the probability distribution of the end-to-end vector. The effect of topological constraint on the chain conformation can be accounted for by a tube-contraction probability density. Furthermore, strain-induced crystallization is considered here as a phase transition, and thus causes a raise in temperature. Consequently it increases the disorder of segmental arrangement in the system. The disorder can be described by an additional entropy term η_θ. Since the three events (changes in the number of microstates due to the chain stretch, the tube contraction and the change in temperature, respectively) are considered independent, the network entropy is therefore given by (Khiêm & Itskov 2018b)

$$\eta = N_c s_{\mathbf{F}}(\mathbf{F}, \Xi) + \eta_\theta(T) = N_c(s_c + s_t) + \eta_\theta(T), \tag{8}$$

where N_c is the number of active chains per unit reference volume of the rubber network, and $s_{\mathbf{F}}$ is the deformation-dependent entropy of the mean chain.

The first part of the chain entropy s_c results from the closed-form of Rayleigh's exact distribution function for the non-Gaussian chain, and can be given by (Khiêm & Itskov 2016)

$$s_c = -k_B n \kappa \ln \frac{\pi r}{n \sin\left(\frac{\pi r}{n}\right)}, \tag{9}$$

where n is the number of chain segments, $r = \bar{\lambda} R$ is the normalized end-to-end distance (after division by the Kuhn length) of the mean chain, R denotes the normalized reference end-to-end distance and $\bar{\lambda}$ is the microscopic stretch. The constant $\kappa = \frac{9}{\pi^2}$ arises from the spring constant of the linear coarse-grained model. k_B is the Boltzmann constant.

The second entropy contribution s_t is induced by the topological constraint, and is written by (Khiêm & Itskov 2016)

$$s_t = -k_B \omega \bar{\upsilon}, \tag{10}$$

where ω is a geometrical parameter of the tube, $\bar{\upsilon}$ is the microscopic tube contraction.

Since segments in the freely jointed chain can fluctuate randomly under temperature change, the third part η_θ can be represented in analogy with the entropy of an ideal gas as follows (Khiêm & Itskov 2018b)

$$\eta_\theta(T) = c_0 \ln \frac{T}{T_0}, \tag{11}$$

where T_0 is the referential temperature and the material constant c_0 represents the heat capacity density (per unit referential volume) at constant deformation.

The internal energy of natural rubber can be further decomposed by

$$U = U_{\mathbf{F}}(\mathbf{F}, \Xi) + U_\theta(T). \tag{12}$$

In our model, the deformation-dependent part of internal energy is only taken into account in the case of crystallization (Khiêm & Itskov 2018b). The second term U_θ due to the raise of temperature is given by (Khiêm & Itskov 2018b)

$$U_\theta = c_0(T - T_0). \tag{13}$$

In view of (2), the temperature alteration due to phase transition can be written as (Khiêm & Itskov 2018b)

$$c_0 \dot{T} = \left(\mathbf{P} : \mathbf{E} - \dot{U}_{\mathbf{F}}\right) - \mathrm{Div} Q + \hat{R}. \tag{14}$$

4 ANALYTICAL HOMOGENIZATION

In Khiêm & Itskov (2016, 2018a, 2018b), we have developed an analytical homogenization scheme for polymeric materials, which permits a transition from the macroscopic level to the scale of molecule. It assumes the existence of an orientational distribution of subnetworks in the polymer that evolves with the microstructural change (Figure 2). A crucial point of this approach is determination of fraction of subnetworks oriented in different directions at a continuum material point. Latest spectacular developments in experimental techniques using mechanochemistry, wide angle X-ray diffraction and calorimetric signals allow direct access to such microstructural information (Ducrot, Chen, Bulters, Sijbesma, & Creton 2014, Brüning, Schneider, Roth, & Heinrich 2015, Le Cam 2018).

4.1 *Analytical network-averaging*

According to the analytical network-averaging concept (Khiêm & Itskov 2016), each directional chain in the network is represented by a representative

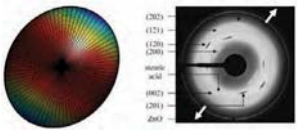

Figure 2. Comparison between the distribution of polymer subnetworks and wide angle X-ray diffraction data under uniaxial loading. The wide angle X-ray diffraction images (b,d) were provided through the courtesy of Bertrand Huneau.

chain confined in a tube undergoing an average-tube stretch and an average-tube contraction.

The spatial distribution function of polymer chains in arbitrary direction can be developed into a series of probability density functions ρ_i related to a set of predefined directions specified by unit vectors E_i ($i = 1, 2, .., m$) as follows

$$\rho(n) = \sum_{i=1}^{m} \frac{1}{m} \cdot \tilde{\rho}_i(n) = \sum_{i=1}^{m} \frac{1}{m} \cdot \rho_i(\theta_i, \varsigma_i, \boldsymbol{E}_i). \quad (15)$$

Therein, m is the number of equidistant collocation points on a half-sphere specifying the deformation-induced anisotropy. Each constituent $\rho_i(\theta_i, \varsigma_i, E_i)$ of the probability density (15) is defined on the basis of an even von Mises-Arnold-Fisher distribution function (Khiêm & Itskov 2017) as

$$\rho_i(\theta_i, \varsigma_i, \boldsymbol{E}_i) = \frac{\varsigma_i}{4\pi \sinh(\varsigma_i)} \cosh(\varsigma_i \cdot \cos\theta_i), \quad (16)$$

where θ_i indicates the angle between the directional unit vector n and the vector $\boldsymbol{E}_i$, ς_i denotes the concentration parameter.

The most general formulation of the concentration parameters can be given at time t by (for the sake of brevity, explicit reference to the material point $\boldsymbol{X}$ is omitted in the response functional)

$$\varsigma_i(t) = \underset{\tau \in (-\infty, t]}{\mathcal{M}} [\mathbf{F}(\tau), \Xi], \quad (17)$$

where $\mathbf{F}(\tau)$ denotes the deformation gradient at time τ in the past and Ξ is an internal variable.

The mesoscopic stretch is evaluated as the root mean square of the macroscopic stretch over the unit sphere by taking the directional chain distribution into account (Khiˆem & Itskov 2018a)

$$\bar{\Lambda} = \sqrt{\sum_{i=1}^{m} \frac{1}{m} \cdot \left((1 - w_i) \frac{I_1}{3} + w_i \Lambda_i^2 \right)}, \quad (18)$$

where θ_i and φ_i are spherical coordinates of the vector n with respect to orthonormal vectors based on the collocation directions $\boldsymbol{E}_i$. $\boldsymbol{I}_1$ denotes the first principal invariant of the right Cauchy-Green tensor $\mathbf{C} = \mathbf{F}^{\mathrm{T}}\mathbf{F}$, and $\Lambda_i^2 = C : \boldsymbol{E}_i \otimes E_i$ is the square of the macro-stretch in direction $\boldsymbol{E}_i$. The fraction of chains w_i aligned in each direction i ($i = 1, 2, .., m$) is expressed by

$$w_i = \frac{{\varsigma_i}^2 - 3\coth(\varsigma_i)\varsigma_i + 3}{{\varsigma_i}^2}. \quad (19)$$

In the next step, the mesoscopic tube contraction is evaluated as the root mean square of the macroscopic tube contraction over the unit sphere. In the same manner as (18), the mesoscopic tube contraction is derived as

$$\bar{\Upsilon} = \sqrt{\sum_{i=1}^{m} \frac{1}{m} \cdot \left((1 - w_i) \frac{I_2}{3} + w_i \Upsilon_i^2 \right)}, \quad (20)$$

where I_2 denotes the second principal invariant of the right Cauchy-Green tensor $\mathbf{C}$ and Υ_i is the macro tube contraction in direction i. It is expressed as $\Upsilon_i^2 = \mathrm{cof}\mathbf{C} : \boldsymbol{E}_i \otimes \boldsymbol{E}_i$, where $\mathrm{cof}\mathbf{C} = \mathbf{C}^{-\mathrm{T}}\det\mathbf{C}$.

4.2 *Mesostretch amplification*

By comparison of different physically-based constitutive models with molecular dynamics simulation of several polymers, it was demonstrated (Khiêm & Itskov 2017) that an additional transition between the mesoscopic and microscopic scales is essential to capture the failure stretch of the polymer network. Accordingly, the micro-stretch is expressed by

$$\bar{\lambda} = \bar{\Lambda}^q, \quad (21)$$

where q is the stretch amplification exponent related to the degree of inhomogeneity of the rubber network.

5 STRAIN INDUCED CRYSTALLIZATION

Phase transition in polymeric materials is governed by the crystallization kinetics. It generally contains two steps: formation of a solid cluster of polymer segments (nucleus) in the amorphous network and growth of such cluster. These steps are referred to as crystallization nucleation and growth, respectively. In this section, we shall derive the evolution of the number of crystallites during cyclic loading of natural rubber and demonstrate the connection between the crystallinity and the fraction of oriented subnetworks w_i in different directions.

5.1 *Crystallization nucleation*

The crystallite is assumed here to be bundle-like with a cylindrical geometry (cf. Candau et al. (2014), Liu et al. (2014) and Gros et al. (2015)). Each crystallite is built by K neighbouring polymer chains. The change in the free energy of a subnetwork due to the nucleation of a crystallite is given by

$$\Delta G = \gamma_t 2Ks + \gamma_s 2\sqrt{\pi Ks}l - Ksl\Delta\Psi_{\mathrm{i}}, \quad (22)$$

where γ_t is the surface tension at the top surfaces of the crystallite. γ_s is the surface tension at the side of the crystallite. $\Delta\Psi_{\mathrm{i}}$ is the difference in bulk free energies between the semicrystalline and the amorphous

subnetworks. s is the cross-section area of a single polymer chain, and l is the length of the crystallite.

Thus, according to the Lauritzen-Hoffman nucleation theory (Hoffman & Lauritzen 1961), the number of molecules K^b in the critical nucleus size can be obtained as

$$K^b = \frac{4\pi\gamma_s^2}{s\Delta\Psi_{\mathrm{i}}^2}. \tag{23}$$

Crystallites with the number of molecules larger than this critical value are likely to grow. The free energy barrier is given in view of (22) by

$$\Delta G^b = \frac{8\pi\gamma_t\gamma_s^2}{\Delta\Psi_{\mathrm{i}}^2}. \tag{24}$$

Therefore, the fraction of chains aligned in each direction can be calculated as

$$w_{\mathrm{i}} = w_{\mathrm{C}} \exp\left(-\frac{8\pi\gamma_t\gamma_s^2}{k_{\mathrm{B}}T\Delta\Psi_{\mathrm{i}}^2}\right), \tag{25}$$

where w_{C} denotes the limit of chain alignment (Toki, Sics, Ran, Liu, Hsiao, Murakami, Senoo, & Kohjiya 2002).

5.2 *Crystallization growth*

Under unloading, some crystallites melt and the sample temperature decreases. Due to the reduction of temperature, mobility of molecules reduces and the secondary crystals grow by aggregation of polymer segments into the critical nuclei (Khiêm & Itskov 2018b) . The probability of the crystallization growth in a direction i is a joint probability of the crystal nucleation P_n and the likelihood P_d that the polymer segments can overcome the diffusion barrier. In other words, the number of secondary crystallites in the direction i, $i = 1, 2, \ldots, m$, is a multiplication of the number of nuclei n_{n} and the number of grown crystallites n_{g} from each nucleus as

$$n_{ci} = n_{\mathrm{n}} \cdot n_{\mathrm{g}}. \tag{26}$$

In view of (25)

$$n_{\mathrm{n}} = n_{\mathrm{U}}\hat{f}\left(\Lambda_{\mathrm{i}}^{\mathrm{c\,max}}\right), \tag{27}$$

where n_{U} is the maximum number of nuclei involved in the crystallization growth and $\hat{f}\left(\Lambda_{\mathrm{i}}^{\mathrm{c\,max}}\right) = \exp\left(-\frac{8\pi\gamma_t\gamma_s^2}{k_{\mathrm{B}}T_0\Delta\Psi_{\mathrm{Ui}}^2\left(\Lambda_{\mathrm{i}}^{\mathrm{c\,max}}\right)}\right)$.

The number of grown crystallites n_{g} can be calculated by subtracting the number of melted segments from the number of segments diffused into the crystal nucleus as

$$n_{\mathrm{g}} = n_{\mathrm{G}}\left[\hat{f}\left(\Lambda_{\mathrm{i}}^{\mathrm{c\,max}}\right) - \hat{f}(\Lambda_{\mathrm{i}})\right]. \tag{28}$$

5.3 *Crystallinity*

The primary crystallinity can be calculated using (25) as

$$\zeta_{\mathrm{b}} = B_{\mathrm{L}} \sum_{i=1}^{m} \exp\left(-\frac{8\pi\gamma_t\gamma_s^2}{k_{\mathrm{B}}T_0\Delta\Psi_{\mathrm{i}}^2(\Lambda_{\mathrm{i}})}\right). \tag{29}$$

The secondary crystallinity is obtained via (26), (27) and (28) as

$$\zeta_{\mathrm{c}} = B_{\mathrm{U}} \sum_{i=1}^{m} \hat{f}(\Lambda_{\mathrm{i}})\left[\hat{f}\left(\Lambda_{\mathrm{i}}^{\mathrm{c\,max}}\right) - \hat{f}(\Lambda_{\mathrm{i}})\right], \tag{30}$$

where B_{U} is the secondary crystallinity constant.

Therefore, the total crystallinity is the sum of the primary and secondary crystallinity

$$\zeta = \zeta_{\mathrm{b}} + \zeta_{\mathrm{c}}. \tag{31}$$

6 RESULTS

In this section, predictive capability of the model in the case of strain-induced crystallization in natural rubber is demonstrated by a comparison with experimental data. First, the model is fitted to uniaxial tension data of natural rubber (Le Cam, Samaca Martinez, Balandraud, Toussaint, & Caillard 2015) to determine its material constants (Fig. 3). Afterwards, the tensile force on the branches of the cross-shaped specimen in the equibiaxial experiment is predicted and plotted versus macroscopic stretch (Fig. 4).

7 CONCLUSIONS

In the current work, we proposed a thermo-micromechanical model capturing strain-induced crystallization in natural rubbers. The model is developed on the basis of the analytical homogenization scheme (Khiêm & Itskov 2018b). Accordingly, the spatial arrangement of polymer chains is driven by crystallization kinetics. It alters the microscopic boundary conditions of the representative chain and induces the thermodynamic irreversibility. The model prediction showed good agreement with both mechanical response and calorimetric analysis of natural rubber.

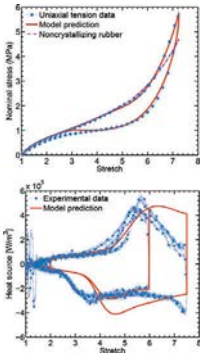

Figure 3. Predictions of the proposed model in the case of strain-induced crystallization in comparison to experimental data of natural rubber undergoing uniaxial tension: stress-stretch response (top), and evolution of heat source (bottom).

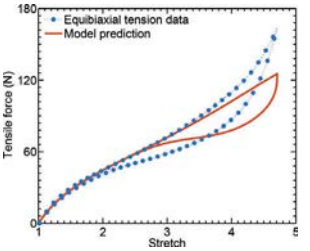

Figure 4. Comparison between model predictions and experimental data of natural rubber in equibiaxial tension.

REFERENCES

Behnke, R., T. Berger, & M. Kaliske (2018). Numerical modeling of time- and temperature-dependent strain-induced crystallization in rubber. *International Journal of Solids and Structures 141-142*, 15–34.

Brüning, K., K. Schneider, S. V. Roth, & G. Heinrich (2015). Kinetics of strain-induced crystallization in natural rubber: A diffusion-controlled rate law. *Polymer 72*, 52–58.

Candau, N., R. Laghmach, L. Chazeau, J.-M. Chenal, C. Gauthier, T. Biben, & E. Munch (2014). Strain-Induced Crystallization of Natural Rubber and Cross-Link Densities Heterogeneities. *Macromolecules 47*(16), 5815–5824.

Chrysochoos, A., V. Huon, F. Jourdan, J. Muracciole, R. Peyroux, & B. Wattrisse (2010). Use of full-field digital image correlation and infrared thermography measurements for the thermomechanical analysis of material behaviour. *Strain 46*, 117–130.

Ducrot, E., Y. Chen, M. Bulters, R. P. Sijbesma, & C. Creton (2014). Toughening elastomers with sacrificial bonds and watching them break. *Science 344*(6180), 186–189.

Germain, P., Q. S. Nguyen, & P. Suquet (1983). Continuum Thermodynamics. *Journal of Applied Mechanics 59* (4b), 1010–1020.

Gros, A., B. Huneau, E. Verron, & M. Tosaka (2019). A physically-based model for strain-induce d crystallization in natural rubber. Part I: Life cycle of a crystallite. *Journal of the Mechanics and Physics of Solids 125*, 164–177.

Gros, A., M. Tosaka, B. Huneau, E. Verron, S. Poompradub, & K. Senoo (2015). Dominating Factor of Strain-induced Crystallization in Natural Rubber. *Polymer 76*, 230–236.

Hoffman, J. D. & J. Lauritzen (1961). Crystallization of Bulk Polymers With Chain Folding: Theory of Growth of Lamellar Spherulites. *Journal of Research of the National Bureau of Standards-A. Physics and Chemistry 65A*(4), 297–336.

Holzapfel, G.-A. (2000). *Non linear solid mechanics - a continuum approach for engineering*. Wiley.

Khiêm, V. N. & M. Itskov (2016). Analytical network-averaging of the tube model: Rubber elasticity. *Journal of the Mechanics and Physics of Solids 95*, 254–269.

Khiêm, V. N. & M. Itskov (2017). An averaging based tube model for deformation induced anisotropic stress softening of filled elastomers. *International Journal of Plasticity 90*, 96–115.

Khiêm, V. N. & M. Itskov (2018a). Analytical network-averaging of the tube model: Mechanically induced chemiluminescence in elastomers. *International Journal of Plasticity 102*, 1–15.

Khiêm, V. N. & M. Itskov (2018b). Analytical network-averaging of the tube model: Strain-induced crystallization in natural rubber. *Journal of the Mechanics and Physics of Solids 116*, 350–369.

Laghmach, R., N. Candau, L. Chazeau, & E. Munch (2015). Phase field modelling of strain induced crystal growth in an elastic matrix. *The Journal of Chemical Physics 142*, 244905.

LeÂ Cam, J.-B. (2018). Strain-induced crystallization in rubber: A new measurement technique. *Strain 54*(1), e12256.

Le Cam, J.-B., J. R. Samaca Martinez, X. Balandraud, E. Toussaint, & J. Caillard (2015). Thermomechanical Analysis of the Singular Behavior of Rubber: Entropic Elasticity, Reinforcement by Fillers, Strain-Induced Crystallizaation and the Mullins Effect. *Experimental Mechanics 55*(4), 771–782.

Le Cam, J.-B. & E. Toussaint (2008). Volume Variation in Stretched Natural Rubber: Competition between Cavitation and Stress-Induced Crystallization. *Macromolecules 41*, 7579–7583.

Liu, D., N. Tian, N. Huang, K. Cui, Z. Wang, T. Hu, H. Yang, X. Li, & L. Li (2014). Extension-induced nucleation under near-equilibrium conditions: The mechanism on the transition from point nucleus to shish. *Macromolecules 47*(19), 6813–6823.

Plagge, J. & M. Klüppel (2018). A Theory Relating Crystal Size, Mechanical Response, and Degree of Crystallization in Strained Natural Rubber. *Macromolecules 51* (10), 3711–3721.

Samaca Martinez, J. R., J.-B. Le Cam, X. Balandraud, E. Toussaint, & J. Caillard (2013a). Mechanisms of deformation in crystallizable natural rubber. Part 1: Thermal characterization. *Polymer 54*(11), 2717–2726.

Samaca Martinez, J. R., J.-B. Le Cam, X. Balandraud, E. Toussaint, & J. Caillard (2013b). Mechanisms of deformation in crystallizable natural rubber. Part 2: Quantitative calorimetric analysis. *Polymer 54*(11), 2727–2736.

Toki, S., I. Sics, S. Ran, L. Liu, B. S. Hsiao, S. Murakami, K. Senoo, & S. Kohjiya (2002). New insights into structural development in natural rubber during uniaxial deformation by in situ synchrotron X-ray diffraction. *Macromolecules 35*(17), 6578–6584.